Conference on Modelling Fluid Flow (CMFF'25)
The 19th International Conference on Fluid Flow Technologies
Budapest, Hungary, August 26-August 29, 2025

Modelling of Parametric Oscillations in Floating Bodies

Erik SILVA FUJIYAMA[1], Josh DAVIDSON[2], Tamás KALMÁR-NAGY[3]

[1] Department of Fluid Mechanics, Faculty of Mechanical Engineering, Budapest University of Technology and Economics. Bertalan Lajos u. 4 - 6, H-1111 Budapest, Hungary. Corresponding Author. E-mail: erik.fujiyama@edu.bme.hu
[2] Basque Center for Applied Mathematics, Mazarredo 14, 48009 Bilbao, Spain. E-mail: jdavidson@bcamath.org
[3] Department of Fluid Mechanics, Faculty of Mechanical Engineering, Budapest University of Technology and Economics. E-mail: kalmar.nagy.tamas@gpk.bme.hu

ABSTRACT

Parametric resonance is a dynamic instability that causes exponential growth in the amplitude of an oscillating system. This study presents a nonlinear Mathieu-type equation model for floating bodies excited by waves, developed to capture parametric resonance in both the heave and pitch degrees of freedom. The model includes nonlinear hydrostatic restoring forces and incorporates position-dependency of the wave excitation forces. Through a nondimensional analysis, a previous model is simplified. A non-cylindrical axisymmetric spar-buoy was used as a test case. The wave excitation forces were calculated for various heave and pitch positions, and interpolated with a third-order polynomial. Simulations showed parametric resonance when the wave frequency is twice the natural frequency of the structure. The results compared favourably to those from a benchmark model with nonlinear Froude-Krylov forces, but achieving a 1000-fold speed increase. On top of this increased computational efficiency, the presented model facilitates analytical approaches, such as perturbation analysis or harmonic balance.

Keywords: Mathieu equation, nonlinear hydrodynamic modelling, parametric resonance, spar buoy, wave-structure interaction

NOMENCLATURE

F_{hr}	$[N]$	hydrostatic restoring force
H	$[m]$	wave amplitude
I	$[Nm]$	inertia moment
I_a	$[Nm]$	added inertia
M_{hr}	$[Nm]$	hydrostatic restoring momentum
R	$[m]$	buoy radius
T	$[s]$	time scale
V	$[m^3]$	submerged volume
Z	$[m]$	length scale for the heave
g	$[m/s^2]$	gravitational acceleration
$a_{i,j}$	$[-]$	nondimensional coefficient for force amplitude
$b_{i,j}$	$[-]$	nondimensional coefficient for moment amplitude
c_a	$[kg]$	radiation damping
cg	$[m]$	center of gravity
$d_{i,j}$	$[-]$	nondimensional coefficient for heave phase
f_e	$[N]$	excitation force amplitude
$f_{i,j}$	$[-]$	nondimensional coefficient for pitch phase
h_0	$[m]$	height of the truncated cone
h_1	$[m]$	height of the cylinder
m	$[kg]$	mass of the floating body
m_a	$[kg]$	added mass
m_e	$[Nm]$	excitation moment amplitude
x_{cb}	$[m]$	center of buoyancy horizontal position
x_{cg}	$[m]$	center of gravity horizontal position
z	$[m]$	heave position
α	$[m]$	buoy angle
η	$[m]$	wave elevation
ω	$[rad/s]$	wave frequency
ω_0	$[rad/s]$	natural frequency
Φ	$[rad]$	length scale for the pitch
ρ	$[kg^3]$	water density
θ_e	$[rad]$	phase angle
φ	$[rad]$	pitch position
ζ	$[m]$	buoy height position

1. INTRODUCTION

Parametric resonance is a dynamic instability that causes exponential growth in the amplitude of an oscillating system. It occurs in differential equations with time-varying coefficients [1]. The most well-known example of such equations is the Mathieu equation, a second-order ordinary differential equation (ODE) with no external forcing and a harmonically time-varying parameter.

Various phenomena, such as the oscillations of floating vessels [2] are described by the Mathieu equation or variants of it [3]. A floating body excited by waves is often described by a Mathieu equation, with an external excitation and damping added. The

time-varying parameter, normally represents a part of the hydrostatic stiffness, and leads to heave-to-pitch instability.

Heave-to-heave instabilities on the other hand, caused by a non constant cross-sectional area in the body, are rarely found in the literature. This type of instability was studied numerically by Jang and Kim in [4] for the case of an Arctic Spar. Lelkes et al. in [5] developed an analytical model to capture the heave-to-heave parametric instability. In the modelling presented in [5], the occurrence of parametric resonance in the heave was not induced by the nonlinear hydrostatic stiffness term, but rather derived from the wave excitation force being dependent on the heave position. This dependency was obtained through the interpolation of the wave excitation force calculated at various positions. Even though positional dependence of hydrodynamic forces was also considered by Rodriguez and Neves in [6], the approach was different: in [6] a Taylor series expansion was applied to a simplified approximation of the force near the equilibrium point. In [7], the model developed in [5] was expanded to also include the pitch. In this paper, an evaluation of the significance of the parameters by a nondimensionalization will be made in the model presented in [7], and simplifications will be made in the interpolations, making the model simper and faster. A model with nonlinear Froude-Krylov forces [8] will be used as the benchmark.

2. ANALYTICAL MODEL FOR PARAMETRIC RESONANCE

In this Section the same procedure that was used in [5] and [7] to model the movement of a spar-buoy excited by harmonic waves will be applied.

In Figure 1, a floating body is shown along with the world coordinate system $\boldsymbol{ij}$. The origin of this system is horizontally aligned with the body's center of gravity (cg) and vertically at the still water level (SWL), which represents the water surface elevation without wave effects. The motion of the body is constrained to the heave DoF z, i.e vertical motion in the $\boldsymbol{j}$ axis, and the pitch DoF φ, i.e rotation around the cg. The wave elevation η is measured relative to the SWL. By convention, the wave propagation direction follows the direction of the $\boldsymbol{i}$ axis.

Only harmonic wave elevations, defined as

$$\eta(t) = H \cdot \cos(\omega t), \tag{1}$$

where H is the wave amplitude and ω is the wave frequency, are considered.

The model proposed by Lelkes et al. and presented in [5] is

$$\begin{aligned}&(m + m_a(\omega))\,\ddot{z} + c_a(\omega)\dot{z} + F_{hr}(z)\\ &= f_e(z,\omega)H\cos(\omega t - \theta_e(z,\omega)).\end{aligned} \tag{2}$$

where m is the mass of the floating body, m_a is the added mass, c_a is the radiation damping, F_{hr} is the hydrostatic restoring force, f_e and θ_e are the wave excitation amplitude coefficient and the phase angle. By expanding Eq. (2) to also include include the pitch degree of freedom, the following coupled system presented in [7] is obtained

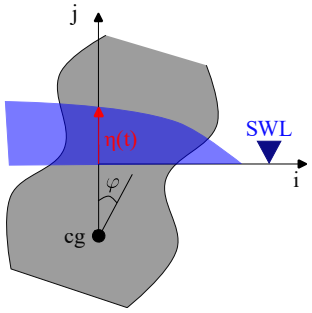

Figure 1. Floating body, wave elevation, and the world coordinate system for two DoFs

$$\begin{aligned}&(m + m_a(\omega))\,\ddot{z} + m_{a2}(\omega)\ddot{\varphi} + c_a(\omega)\dot{z} + c_{a3}(\omega)\dot{\varphi}\\ &+ F_{hr}(z,\varphi) = f_e(z,\varphi,\omega)H\cos(\omega t - \theta_e(z,\varphi,\omega)),\end{aligned} \tag{3}$$

$$\begin{aligned}&(I + I_a(\omega))\,\ddot{\varphi} + I_{a2}(\omega)\ddot{z} + c_{a2}(\omega)\dot{\varphi} + c_{a4}(\omega)\dot{z}\\ &+ M_{hr}(z,\varphi) = m_e(z,\varphi,\omega)H\cos(\omega t - \theta_{e2}(z,\varphi,\omega)),\end{aligned} \tag{4}$$

where I is the rotational inertia, I_a is the added rotational inertia, M_{hr} is the hydrostatic restoring moment, and m_e is the wave excitation amplitude moment coefficient.

3. CASE STUDY

In this Section, a test case is presented to evaluate the performance of the parametric excitation model (Eqs. 3 and 4). The test case is generic, not containing a mooring system, as the primary focus of the model is the wave excitation force. Additionally, conditions of infinite water depth are considered.

3.1. The floating body

The floating body considered in the test case is an axisymmetric spar-buoy, similar to the one examined in [5] and [7]. It consists of a truncated cone and a cylindrical extension, as illustrated in Figure 2. The exact shape of the spar-buoy is defined by:

$$f(\zeta) = \begin{cases} R_1 & \text{if } -\frac{h_0}{2} + h_1 \le \zeta \le \frac{h_0}{2}, \\ R_0 + \zeta\tan(\alpha) & \text{if } -\frac{h_0}{2} \le \zeta \le \frac{h_0}{2}, \\ 0 & \text{otherwise.} \end{cases} \tag{5}$$

The physical parameters of the spar-buoy shown in Fig. 2 and their corresponding values are $\alpha = 0.197\ [rad]$, $R_0 = 3\ [m]$, $h_0 = 10\ [m]$, $h_1 = 15\ [m]$, $R_1 = 2\ [m]$, $z_{cg} = 16\ [m]$, $m = 2.95 \cdot 10^5\ [kg]$, and $I = 1.18 \cdot 10^7\ [kg \cdot m^2]$. The water density is $\rho = 1025\ [kg/m^3]$ and the gravitational acceleration is $g = 9.806\ [m/s^2]$.

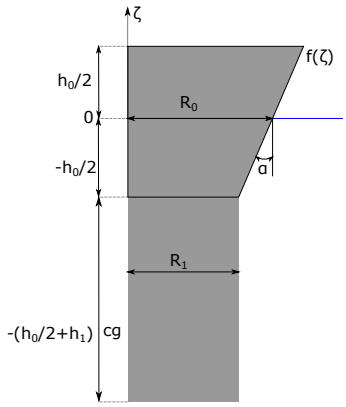

Figure 2. Section of the spar-buoy geometry

3.2. Modelling the test case

With g and ρ given in Subsection 3.1, the hydrostatic restoring terms F_{hr} and M_{hr} are calculated based on the body geometry with

$$F_{hr}(z,\varphi) = \rho_{water} g \Delta V(z,\varphi), \tag{6}$$

where $\Delta V(z) = V(z) - V(0)$, $V(z)$ being the submerged volume, and

$$M_{hr}(z,\varphi) = \rho g \Delta V(z,\varphi) \cdot (x_{cb}(z,\varphi) - x_{cg}), \tag{7}$$

where x_{cb} is the horizontal position of the center of buoyancy, and x_{cg} is the horizontal position of the center of gravity.

In this case $F_{hr}(z,\varphi)$ and $M_{hr}(z,\varphi)$ are calculated numerically with the CAD software FreeCAD [9]. The values for F_{hr} and M_{hr} are determined for a set of discrete pitch angles ranging from -0.21 $[rad]$ to 0.21 $[rad]$, with a step size of 0.07 $[rad]$, and for heave displacements from -4 $[m]$ to 4 $[m]$, with a step size of 1 $[m]$.

An interpolation is then performed on the generated dataset to describe F_{hr} and M_{hr} continuously, employing polynomial functions of the heave z and pitch φ displacement. The resulting polynomial expressions are

$$F_{hr}(z,\varphi) = \rho g \Delta V(z,\varphi) \approx \sum_{1 \le i+j \le 3} r_{i,j} z^i \varphi^j, \tag{8}$$

$$M_{hr}(z,\varphi) = \rho g \Delta V(z,\varphi)(x_{cb}(z,\varphi) - x_{cg}) \approx \sum_{1 \le i+j \le 3} s_{i,j} z^i \varphi^j, \tag{9}$$

where $r_{i,j}$ are the hydrostatic restoring coefficients for the heave obtained from the polynomial interpolation, and $s_{i,j}$ are the hydrostatic restoring coefficients for the pitch obtained from the polynomial interpolation.

The calculation of the wave excitation coefficients f_e, m_e, θ_e, and θ_{e2} is done with the open-source boundary element solver NEMOH [10], which computes first-order hydrodynamic coefficients, such as added mass, radiation and excitation forces in the frequency domain.

A model with nonlinear Froude-Krylov forces that does not consider the diffraction force [8] will be used as the benchmark, so this component will also be neglected in the present study. This approach is common for bodies that are small relative to the wavelength [11], and it can be easily configured with NEMOH.

In this test case, the wave excitation coefficients are computed for the same discrete displacements used in the hydrostatic restoring terms. The wave excitation terms are also interpolated with polynomial functions, yielding the following expressions

$$f_e = \sum_{0 \le i+j \le 3} a_{i,j}(\omega) z^i \varphi^j, \; \theta_e = \sum_{0 \le i+j \le 1} d_{i,j}(\omega) z^i \varphi^j, \tag{10}$$

$$m_e = \sum_{0 \le i+j \le 3} b_{i,j}(\omega) z^i \varphi^j, \; \theta_{e2} = \sum_{0 \le i+j \le 2} f_{i,j}(\omega) z^i \varphi^j \tag{11}$$

where $a_{i,j}$, $d_{i,j}$, $b_{i,j}$, and $f_{i,j}$ are the coefficients obtained from the polynomial interpolation.

The radiation and added mass coefficients m_a, m_{a2}, I_a, I_{a2}, c_a, c_{a2}, c_{a3} and c_{a4}, in Eqs. (3) and (4), are also computed using NEMOH.

The cross terms $m_{a2}(\omega)$, $c_{a3}(\omega)$, $I_{a2}(\omega)$ and $c_{a4}(\omega)$, calculated for NEMOH were negligible, being over four orders of magnitude smaller than the other coefficients. This outcome is expected for an axisymmetric body, so they were neglected from the model in this test case.

The radiation damping coefficients depend on the frequency of the body motion. In a linear model, a body oscillates at the same frequency as the excitation. In a nonlinear model, such as the parametric excitation model, this is not always the case. However, in the present test case, following Lelkes et al. in [5], the radiation damping considered will be with the excitation frequency. Even though this simplification introduces error, the wave excitation forces, which are the primary focus of the model, are not affected. Simplifications of this kind are not uncommon in literature, as seen in works such as [12, 13, 14], where the radiation damping was similarly simplified to focus on other specific aspects of the analysis.

4. NONDIMENSIONALIZATION

In order to better understand the significance of the parameters in the model, and remove terms that do not alter the results, the 2-DoF model is nondimensionalized. The nondimensional variables are defined as follows

$$\tilde{t} = \frac{t}{T}, \tilde{z} = \frac{z}{Z}, \tilde{\varphi} = \frac{\varphi}{\Phi}. \tag{12}$$

The length and angle scales Z and Φ are defined so that $\tilde{z}$ and $\tilde{\varphi}$ have a validity region between -1 and 1. As the validity region of the model is defined as $|z| \leq 4$ $[m]$ and $|\varphi| \leq 0.21$ $[rad]$ (as stated in Section 3),

$$Z = 4\ [m],\ \Phi = 0.21\ [rad]. \tag{13}$$

The time scale T is defined as

$$T = \sqrt{\frac{m + m_a(\omega)}{r_{1,0}}}. \tag{14}$$

The nondimensional equations become

$$\ddot{\tilde{z}} + \alpha_3(\omega)\dot{\tilde{z}} + \sum_{1\leq i+j\leq 3} \gamma_{i,j}(\omega)\tilde{z}^i\tilde{\varphi}^j = \cos\left(\nu\tilde{t} - \sum_{0\leq i+j\leq 1} \xi_{i,j}(\omega)\tilde{z}^i\tilde{\varphi}^j\right) \sum_{0\leq i+j\leq 3} \beta_{i,j}(\omega)\tilde{z}^i\tilde{\varphi}^j, \tag{15}$$

$$\ddot{\tilde{\varphi}} + \alpha_5(\omega)\dot{\tilde{\varphi}} + \sum_{1\leq i+j\leq 3} \zeta_{i,j}(\omega)\tilde{z}^i\tilde{\varphi}^j = \cos\left(\nu\tilde{t} - \sum_{0\leq i+j\leq 2} \chi_{i,j}(\omega)\tilde{z}^i\tilde{\varphi}^j\right) \sum_{0\leq i+j\leq 3} \mu_{i,j}(\omega)\tilde{z}^i\tilde{\varphi}^j, \tag{16}$$

where the nondimensional parameters are

$$\begin{aligned}
&\alpha_3(\omega) = \frac{c_3}{\sqrt{(m + m_a(\omega))r_{1,0}}},\\
&\alpha_5(\omega) = \frac{c_5\sqrt{m + m_a(\omega)}}{(I + I_a(\omega))\sqrt{r_{1,0}}},\\
&\gamma_{i,j}(\omega) = \frac{1}{r_{1,0}} r_{i,j} Z^{i-1}\Phi^i,\ \beta_{i,j}(\omega) = \frac{H}{r_{1,0}} a_{i,j} Z^{i-1}\Phi^i,\\
&\zeta_{i,j}(\omega) = \frac{T^2}{I + I_a(\omega)} s_{i,j} Z^i \Phi^{i-1},\\
&\mu_{i,j}(\omega) = \frac{HT^2}{I + I_a(\omega)} b_{i,j} Z^i \Phi^{i-1},\\
&\nu(\omega) = \omega\sqrt{\frac{m + m_a(\omega)}{r_{1,0}}},\\
&\xi_{i,j} = d_{i,j} Z^i \Phi^j,\ \chi_{i,j} = f_{i,j} Z^i \Phi^j.
\end{aligned} \tag{17}$$

The restoring parameters are now functions of ω. To estimate their orders of magnitude, their values for $\omega = 1.9$ $[rad/s]$ are provided in Eq. 18 and Table 1

$$\alpha_3 = 0.03,\ \alpha_5 = 0.83,\ \nu = 2. \tag{18}$$

The nondimensional coefficients $\gamma_{i,j}$ and $\zeta_{i,j}$ correspond to the hydrostatic restoring coefficients $r_{i,j}$ and $s_{i,j}$. The coefficients $\beta_{i,j}$, $\mu_{i,j}$, $\xi_{i,j}$ and $\chi_{i,j}$ relate to the wave excitation coefficients $a_{i,j}$, $b_{i,j}$, $d_{i,j}$ and $f_{i,j}$, while α_3 and α_5 correspond to the radiation damping terms c_3 and c_5.

i,j	0, 0	1, 0	2, 0	3, 0	1, 0
$\gamma_{i,j}$	0	0.21	-0.012	$2.26 \cdot 10^{-4}$	$4.67 \cdot 10^{-6}$
$\zeta_{i,j}$	0	$-4.42 \cdot 10^{-9}$	$-2.41 \cdot 10^{-9}$	$1.8 \cdot 10^{-10}$	3.61
$\beta_{i,j}$	0.051	-0.02	-0.01	-0.002	$7.93 \cdot 10^{-6}$
$\mu_{i,j}$	0.01	-0.004	-0.002	$-3.84 \cdot 10^{-4}$	$1.56 \cdot 10^{-6}$
$\xi_{i,j}$	$2.6 \cdot 10^{-5}$	$7.06 \cdot 10^{-4}$	0	0	1.84
$\chi_{i,j}$	-1.57	$9.16 \cdot 10^{-5}$	$-1.56 \cdot 10^{-4}$	0	1.05
i,j	0, 2	0, 3	1, 1	2, 1	1, 2
$\gamma_{i,j}$	-2.28	$1.08 \cdot 10^{-5}$	$-8.43 \cdot 10^{-7}$	$4.63 \cdot 10^{-8}$	0.36
$\zeta_{i,j}$	$-8.76 \cdot 10^{-6}$	7.65	-0.77	0.061	$2.21 \cdot 10^{-6}$
$\beta_{i,j}$	0.017	$-8.54 \cdot 10^{-6}$	$6.66 \cdot 10^{-6}$	$-1.23 \cdot 10^{-5}$	-0.001
$\mu_{i,j}$	0.003	$-1.68 \cdot 10^{-6}$	$1.31 \cdot 10^{-6}$	$-2.43 \cdot 10^{-6}$	$-2.38 \cdot 10^{-4}$
$\xi_{i,j}$	0	0	0	0	0
$\chi_{i,j}$	$-1.49 \cdot 10^{-4}$	0	-0.34	0	0

Table 1. Nondimensional polynomial approximation coefficients for hydrostatic restoring terms ($\gamma_{i,j}$ and $\zeta_{i,j}$), and wave excitation terms ($\beta_{i,j}$ and $\mu_{i,j}$)

The nondimensional coefficients $\gamma_{0,1}$, $\gamma_{1,1}$, $\gamma_{2,1}$, $\zeta_{1,0}$, $\zeta_{2,0}$, $\zeta_{3,0}$, $\zeta_{0,2}$, and $\zeta_{1,2}$ in Table 1 have small values. So a polynomial interpolation for the hydrostatic restoring forces was conducted by setting the coefficients corresponding to these small-valued nondimensional coefficients to zero. The threshold for a coefficient to be deemed small was chosen as $2.26 \cdot 10^{-4}$. This choice was made because it was observed that the term $\gamma_{3,0}$ was the smallest coefficient that still significantly affected the interpolation.

With these small terms set to zero, we recalculate the dimensional parameters $r_{i,j}$ and $s_{i,j}$ in this simplified manner. The results are shown in Table 2.

i,j	1, 0	2, 0	3, 0	0, 1
$r_{i,j}$ (SI)	$2.83 \cdot 10^5$	$-1.93 \cdot 10^4$	434	0
$s_{i,j}$ (SI)	0	0	0	$-2.08 \cdot 10^7$
i,j	0, 2	0, 3	1, 1	2, 1
$r_{i,j}$ (SI)	$-2.59 \cdot 10^6$	0	0	0
$s_{i,j}$ (SI)	0	$-4.42 \cdot 10^7$	$5.29 \cdot 10^7$	$-4.97 \cdot 10^5$
i,j	1, 2			
$r_{i,j}$ (SI)	$4.92 \cdot 10^5$			
$s_{i,j}$ (SI)	0			

Table 2. Hydrostatic restoring coefficients obtained from the polynomial interpolation that set small terms to zero

By comparing the results of the interpolation with the values from Table 2 to the one with the original ones, the difference between the two interpolations across the considered range of $|z| \leq 4$ $[m]$ and $|\varphi| \leq 0.21$ $[rad]$ was never bigger than 10^{-10}. This is negligible, considering that $|\bar{F}_{hr}| = 5.9 \cdot 10^5$ $[N]$ and $|\bar{M}_{hr}| = 2.57 \cdot 10^6$ $[Nm]$.

The same procedure was applied to the wave excitation coefficients and led to the values in Table 3.

5. RESULTS

In this Section, the results from the test case detailed in Section 3 with the simplifications from Section 4 are presented and compared to a model with NLFK forces.

The equations for the presented model Eqs. (3) and (4) are solved numerically using the NDSolve function in Wolfram Mathematica 14.1 with its default settings, and the equations for the model with

i,j	0,0	1,0	2,0	3,0
$a_{i,j}$ (SI)	$5.89 \cdot 10^4$	-5897	-722	-34.2
$b_{i,j}$ (SI)	$2.61 \cdot 10^6$	$-519 \cdot 10^5$	$3.23 \cdot 10^4$	1322
i,j	0,2	1,2		
$a_{i,j}$ (SI)	$4.27 \cdot 10^5$	-7481		
$b_{i,j}$ (SI)	$5.84 \cdot 10^6$	$6.15 \cdot 10^5$		
i,j	0,0	0,1	1,1	
$d_{i,j}$ (SI)	$-2.54 \cdot 10^{-5}$	8.7	0	
$f_{i,j}$ (SI)	-1.57	4.94	-0.41	

Table 3. Wave excitation coefficients obtained from the polynomial interpolation that set small terms to zero

NLFK forces, were solved in Matlab R2021a, using the toolbox developed by Giorgi et al. in [8].

The natural frequency ω_0 is also found numerically, by running a simulation without the external excitation. It is critical to note that the validity region of this parametric excitation model is limited to the range over which the excitation and restoring force coefficients were computed, $|z| \leq 4$ $[m]$, and $|\varphi| \leq 0.21$ $[rad]$.

By numerically solving Eqs. (3) and (4) with these simplified interpolations and comparing to their solution with the initial interpolation, the difference was of the order of 10^{-4}. However, with the simplified interpolations, the running time to obtain the interpolation and perform a simulation of 1000 periods went from 1.94 seconds to 0.27 seconds . So neglecting the small terms does not affect the results significantly, while making the code run faster. As for each simulated frequency, a new interpolation for the wave excitation coefficients is necessary, when evaluating multiple frequencies, the difference in time becomes more significant.

The plots in Figures 3 and 4 show the oscillation amplitude in response to a range of input wave frequencies and amplitudes. The RMS of the displacement time series, scaled by the square root of 2 serves as the measure of amplitude for both heave and pitch motions. This RMS is computed over the last 64 wave periods of the simulation to ensure that motions have reached steady-state.

In Fig. 3 these are shown for the region where heave parametric resonance occurs, while in Fig. 4 for the region where the pitch parametric resonance occurs. At a first view, the contour plots indicate a good match between the models.

In Figures 5 and 6, the time series for Point C in Fig. 3 and Point D in Fig. 4 are plotted. For the parametric excitation model, the amplitude grows faster and larger than for the model with NLFK forces, with a difference of around 20% in the amplitudes. The results also appear slightly off-phase. These differences were also noted for the 1-DoF results in [5].

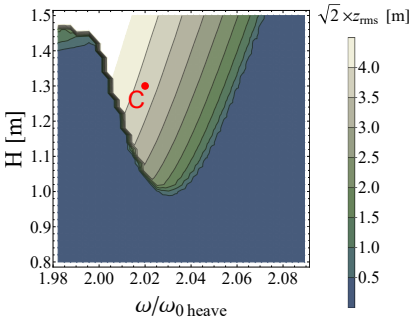

(a) RMS amplitudes for heave from the parametric excitation force model

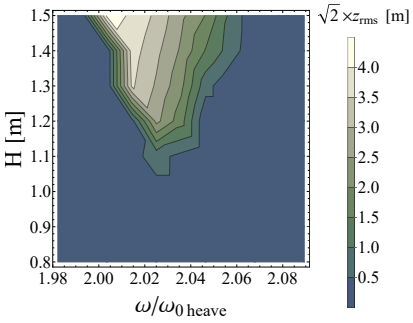

(b) RMS amplitudes for heave from the model with NLFK forces

Figure 3. Contour plots of steady-state amplitudes of the buoy's oscillations in the heave parametric resonance region

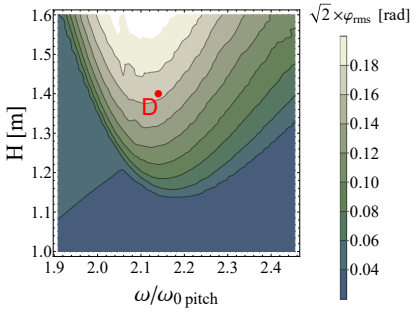

(a) RMS amplitudes for pitch from the parametric excitation force model

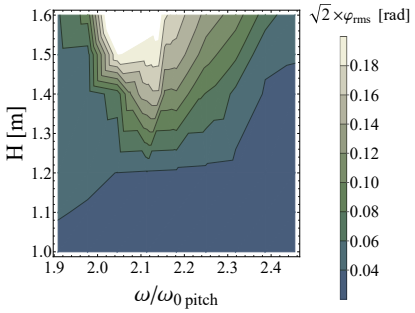

(b) RMS amplitudes for pitch from the model with NLFK forces

Figure 4. Contour plots of steady-state amplitudes of the buoy's oscillations in the pitch parametric resonance region

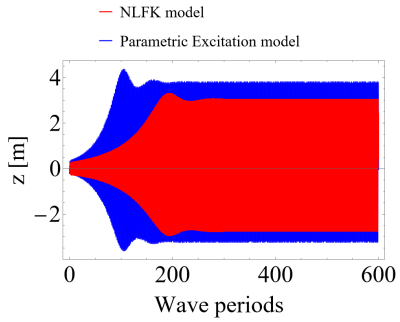

(a) Transient heave oscillations

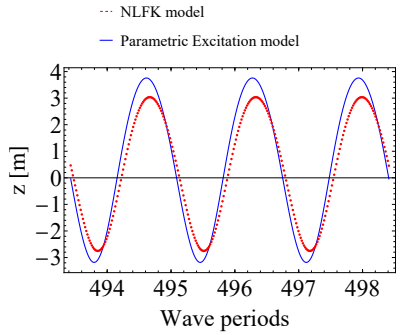

(b) Steady state heave oscillations

Figure 5. Comparison of time series between the parametric excitation model and the model with NLFK forces for the input wave conditions at Point C in Fig. 3: $\frac{\omega}{\omega_{0heave}} = 2.02$ **and** $H = 1.3$ **[**m**]**

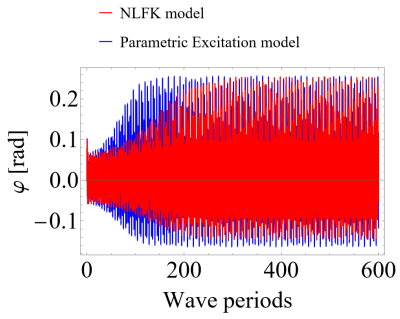

(a) Transient pitch oscillations

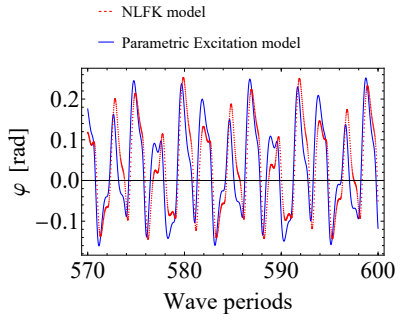

(b) Steady state pitch oscillations

Figure 6. Comparison of time series between the parametric excitation model and the model with NLFK forces for the input wave conditions at Point D in Fig. 4: $\frac{\omega}{\omega_{0pitch}} = 2.14$ **and** $H = 1.4$ **[**m**]**

6. CONCLUSION

In this study, a nondimensional analysis was applied to a previously presented model for a floating body that was able to capture parametric resonance, while being computationally efficient. This modelling approach, with an interpolated parametric excitation is much more computationally efficient than models where the excitation forces are calculated by numerical integration at each step.

By nondimensionalising the system of equations, it was possible to have a better understanding on the significance of the parameters of the model. It was observed that some parameters were negligible, which allowed for the model to be simplified by neglecting them in the interpolation. This simplification did not alter the results, but made the model run much faster.

One important consideration for further studies is that the models presented in this article, calculate the radiation forces as linearly proportional to the body velocity, with the radiation force coefficient derived considering that the body oscillates at the same frequency as the waves. This is a common approach used for single-frequency waves, which is a simplification of the more general convolution integral required in multi-frequency wave spectra [15] [16]. However, as explained in Section 5, in the regions where the parametric resonance occurs, the body oscillates at half of the wave frequency, thus the applied radiation coefficient considers the wrong oscillation frequency. This is something that shall be corrected in an extension of the model to work with polychromatic waves, as the complete convolution integral for the radiation forces must be used for that case.

ACKNOWLEDGEMENTS

The research reported in this paper is part of project no. TKP-6-6/PALY-2021. Project no. TKP-6-6/PALY-2021 has been implemented with the support provided by the Ministry of Culture and Innovation of Hungary from the National Research, Development and Innovation Fund, financed under the TKP2021-NVA funding scheme.

This work has been supported by the Hungarian National Research, Development and Innovation Fund under contract NKFI K 137726. The research reported in this paper and carried out at BME has been supported by the ÚNKP-22-3 New National Excellence Program of the Ministry for Culture and Innovation from the source of the National Research, Development and Innovation Fund.

Erik Silva Fujiyama is funded by the Tempus Public Foundation through the Stipendium Hungaricum Programme.

Josh Davidson is funded by MCIN and by the European Union NextGenerationEU/PRTR-C17.I1, as well as by IKUR Strategy under the collaboration agreement between Ikerbasque Foundation and BCAM on behalf of the Department of Education of the Basque Government.

REFERENCES

[1] Nayfeh, A. H., and Mook, D. T., 2008, *Nonlinear oscillations*, John Wiley & Sons.

[2] Daniel, D. J., 2020, "Exact solutions of Mathieu's equation", *Progress of Theoretical and Experimental Physics*, Vol. 2020 (4), p. 043A01.

[3] Kovacic, I., Rand, R., and Mohamed Sah, S., 2018, "Mathieu's equation and its generalizations: overview of stability charts and their features", *Applied Mechanics Reviews*, Vol. 70 (2).

[4] Jang, H., and Kim, M., 2019, "Mathieu instability of Arctic Spar by nonlinear time-domain simulations", *Ocean Engineering*, Vol. 176, pp. 31–45.

[5] Lelkes, J., Davidson, J., and Kalmár-Nagy, T., 2021, "Modelling of Parametric Resonance for Heaving Buoys With Position-Varying Waterplane Area", *Journal of Marine Science and Engineering*, Vol. 9 (11), p. 1162, URL `https://doi.org/10.3390/jmse9111162`.

[6] Rodríguez, C. A., and Neves, M. A., 2012, "Nonlinear instabilities of spar platforms in waves", *International Conference on Offshore Mechanics and Arctic Engineering*, American Society of Mechanical Engineers, Vol. 44915, pp. 605–614.

[7] Fujiyama, E. S., Lelkes, J., Kalmár-Nagy, T., and Davidson, J., 2025, "A Computationally Efficient Analytical Modelling Approach for Parametric Oscillations in Floating Bodies", *In Review*.

[8] Giorgi, G., Bracco, G., and Mattiazzo, G., 2021, "NLFK4ALL: An open-source demonstration toolbox for computationally efficient nonlinear Froude-Krylov force calculations", *14th WCCM-ECCOMAS Congress*, Vol. 2020, pp. 1–12.

[9] Machado, F., Malpica, N., and Borromeo, S., 2019, "Parametric CAD Modeling for open source scientific Hardware: Comparing Openscad and Freecad Python Scripts", *PLOS ONE*, Vol. 14 (12), p. e0225795, URL `https://doi.org/10.1371/journal.pone.0225795`.

[10] Babarit, A., and Delhommeau, G., 2015, "Theoretical and numerical aspects of the open source BEM solver NEMOH", *11th European Wave and Tidal Energy Conference (EWTEC2015)*, Nantes, France, Proceedings of the 11th European Wave and Tidal Energy Conference, pp. 6–11, URL `https://hal.archives-ouvertes.fr/hal-01198800`.

[11] Folley, M., 2016, *Numerical modelling of wave energy converters: state-of-the-art techniques for single devices and arrays*, Academic Press.

[12] Davidson, J., and Kalmár-Nagy, T., 2020, "A real-time detection system for the onset of parametric resonance in wave energy converters", *Journal of Marine Science and Engineering*, Vol. 8 (10), p. 819.

[13] Gavassoni, E., Gonçalves, P. B., and Roehl, D. M., 2014, "Nonlinear vibration modes and instability of a conceptual model of a spar platform", *Nonlinear Dynamics*, Vol. 76 (1), pp. 809–826.

[14] Hong, Y.-P., Lee, D.-Y., Choi, Y.-H., Hong, S.-K., and Kim, S.-E., 2005, "An experimental study on the extreme motion responses of a spar platform in the heave resonant waves", *Proceedings of the Fifteenth International Offshore and Polar Engineering Conference. Seoul, Korea*, pp. 225–232.

[15] Cummins, W., 1962, "The impulse response function and ship motions", *Tech. rep.*, Department of the Navy, David W. Taylor Model Basin, Hydromechanics Laboratory, Research and Development Report.

[16] Ahmed, A., Yang, L., Huang, J., Shalaby, A., Datla, R., Zuo, L., and Hajj, M., 2024, "Performance characterization and modeling of an oscillating surge wave energy converter", *Nonlinear Dynamics*, pp. 1–19.